CHAPTER - V

STRUCTURAL STABILITY AND ELECTROCHEMICAL PERFORMANCE OF W-DOPED PLATINUM ALLOY NANO PARTICLES FOR SEAWATER ELECTROLYSIS ON ALCOHOL OXIDATION IN NON-MEMBRANE FUEL CELL SYSTEMS

5.1 INTRODUCTION

The treatment of effluents from remediation process of contaminated sediments requires the development and application of green technologies aimed at minimizing waste production and mitigating the negative impact with the adoption of environmentally-friendly chemicals. The development of electrogeneration of seawater on membraneless ethanol fuel cell (MLEFC) has been the target of many researchers, because ethanol is a liquid fuel which can be easily stored, handled and produced in large quantity from biomass through a fermentation process (Adamson et al, 2000; McNicol et al, 1999; Hart et al, 2000; Kiso et al, 1998). Despite all efforts devoted to the MLEFC development, there still remain problems in terms of efficiency and power density due to slow kinetics of the ethanol oxidation reaction at the anode will leads to high over potentials in the presence of seawater electrolyte.

Pt is known to activate the dissociative adsorption of ethanol at an appreciable rate. The main problem is that ethanol oxidation at a platinum electrode is a self-poisoning reaction, since strongly adsorbed CO and CH_3COOH are produced by electrooxidation of ethanol (Beden et al, 1981; Hamnett, 1997; Burnstein et al, 1997). To promote the ethanol electrooxidation at platinum, modification of the catalyst surface has been made by the addition of a second metal to platinum (Chan et al, 2004;

Rivera et al, 2004; Xiong et al, 2002). Bimetallic Pt−Sn electrocatalysts lead to higher activities towards ethanol oxidation (Lamy et al, 2004; Vigier et al, 2004).Due to the strong adsorption of CO onto the Pt surface, the hydrogen adsorption-desorption of the Pt was completely blocked in the hydrogen region; indicating the presence of a saturated CO adlayer (Choi et al, 2003). Pure Pt/C catalyst (Fig. 5.4b) does not behave as a very good anode for ethanol electro-oxidation due to its poisoning by strongly adsorbed intermediates such as CO_{ads} (Vigier et al, 2004).

The Pt–Sn/C binary metallic catalyst is commonly accepted as the best electrocatalyst for ethanol oxidation due to its high CO tolerance, which can be achieved via its electronic effects and bifunctional mechanisms (Gasteiger et al, 1993; Yajima et al, 2004) that improve the catalytic activities of electrochemical reactions. However, controversy exists concerning the real improvement of the ethanol electrooxidation reaction.

Despite the controversies, recent studies have shown that the Pt–Sn–W/C (Moreno et al, 2009; Ahn et al, 2010) catalyst has a dramatic effect on its electrocatalytic activity. Moreno et al, (2009) pointed out that tin and tungsten atoms either form an alloy with platinum or exist as amorphous oxide phases. The presence of OH_{ads} species in large amounts is necessary for the complete oxidation of poisoning intermediates such as CH_x and CO (Ribeiro et al, 2007).

The enhanced activity of the ternary catalyst is due to the promoting effect of the second or third elements added to Pt. In the present study, we evaluated the catalytic activity for ethanol oxidation reaction (EOR) by incorporating W into Pt–Sn/VC catalysts in MLEFC.

5.2 EXPERIMENTAL

5.2.1 Materials

The metal precursors used for the preparation of electrocatalysts were $H_2PtCl_6.6H_2O$ (from Sigma Aldrich), $SnCl_3.3H_2O$ (from Sigma Aldrich), and WCl_6 (from Sigma Aldrich). Vulcan XC-72R carbon black (from Cabot Corp.,) was used as a support for the catalysts. Graphite plates (from E-TEK) were used as substrates for the catalyst to prepare the electrodes. Ethylene glycol (from Merck) was used as the solvent and reduction agent. Nafion® (DE 521, DuPont USA) dispersion was used to make the catalyst ink. Ethanol (from Merck), sodium perborate (from Riedel), H_2SO_4 (from Merck) and seawater were used as the fuel, the oxidant and as the electrolyte for electrochemical analysis, respectively. All the chemicals were of analytical grade. Pt/VC (40-wt%, from E-TEK) was used as the cathode catalyst.

5.2.2 Catalyst Preparation

Carbon-supported catalysts containing Pt, Sn and W with different atomic ratios were synthesized employing ethylene glycol (EG) as a reactant and reducing agent together with citric acid (CA) in line with the Pechini methodology (Ribeiro et al, 2007; Pechini, 1967; Bonesi et al, 2013). The Pt, Sn and W precursors were prepared separately by employing metallic salts, namely, $H_2PtCl_6.6H_2O$, $SnCl_2.3H_2O$ and WCl_6, dissolved in a mixture of EG and CA at 70 °C and the mixture was kept under vigorous stirring for 2–3 h composing a polyester network that contains the metallic ions homogeneously distributed. The CA/EG/metal molar ratio is 4:16:1 for all the polymeric precursors. It appears that the citric chelate helps to prevent particle aggregation in a certain extent and induce nanoparticles to get high dispersion.

To obtain the supported catalysts, appropriate amounts of the polymeric precursors were dissolved in ethanol and a calculated amount of the functionalized carbon black support was added. Finally, the mixture precursor solution/carbon was homogenized in an ultrasonic bath and then calcinated at different temperatures under an air atmosphere, using a temperature program reaching 400 °C to eliminate the excess carbon (Ribeiro et al, 2007).

For comparison, the monometallic Pt/VC, and bimetallic Pt–Sn/VC and Pt–W/VC catalysts were synthesized under the same conditions. The electrocatalytic mixtures and atomic ratios were $Pt_{60}Sn_{30}W_{10}$/VC, $Pt_{60}Sn_{20}W_{20}$/VC, $Pt_{60}Sn_{10}W_{30}$/VC, $Pt_{50}Sn_{50}$/VC, $Pt_{50}W_{50}$/VC and Pt_{100}/VC. The nominal loading of metals in the electrocatalysts was 40 %wt and rest 60 %wt was carbon.

5.2.3 Physical Characterization

The morphology of the dispersed catalysts was examined using TEM (Philips CM 12 Transmission Electron Microscope). The particle size distribution and mean particle size were also evaluated using TEM. The crystal structure of the synthesized electrocatalysts was characterized by powder X-ray diffraction (XRD) using a Rigaku multiflex diffractometer (model RU-200 B) with Cu-$K_{\alpha 1}$ radiation source ($\lambda_{K\alpha 1}$ = 1.5406 A^o) operating at room temperature. The tube current was 40 mA with a tube voltage of 40 kV. The 2θ angular regions between 20º and 90º were recorded at a scan rate of 5° min^{-1}. The mean particle size analyzed from TEM is verified by determining the crystallite size from XRD pattern using Scherrer formula. Pt (2 2 0) diffraction peak was selected to calculate crystallite size and lattice parameter of platinum. According to Scherrer's equation (Radmilovic et al., 1995)

$$d = \frac{0.9\lambda_{K\alpha 1}}{ß_{2\theta} \cos \theta_{max}} \qquad (5.1)$$

Where d is the average crystallite size, θ_{max} is the angle at the position of the peak maximum, $ß_{2\theta}$ is the width of the peak (in radians), 0.9 is the shape factor for spherical crystallite and $\lambda_{K\alpha 1}$ is the wavelength of X-rays used. The lattice parameters of the catalysts were estimated according to equation 5.2 (Radmilovic et al., 1995):

$$a = \frac{\sqrt{2}\ \lambda_{K\alpha 1}}{\text{Sin}\ \theta_{max}} \qquad (5.2)$$

Where a, is the lattice parameter (nm) and all the other symbols have the same meanings as in equation 5.1 (Beyan et al., 2013). The atomic ratio of the catalysts was determined by an energy dispersive X-ray (EDX) analyzer, which was integrated with the TEM instrument.

5.2.4 Electrochemical Measurement

Electrochemical studies of the electrocatalysts were carried out using the thin porous coating technique (Colmati et al., 2007). All electrochemical measurements were performed on an electrochemical workstation (CH Instruments, model CHI6650, USA) interfaced with a personal computer using the CHI software, at room temperature. A common three-electrode electrochemical cell using cyclic voltammetry (CV) and chronoamperometry (CA) techniques was used for the measurements. Catalyst coated glassy carbon electrode (GCE, 3 mm diameter and 0.071 cm^2 of electrode area, from CHI, USA) was used as the working electrode and platinum foil was used as the counter electrode. Ag/AgCl in saturated KCl was used as the reference electrode (RHE).

The working electrode was prepared by applying catalyst ink made of 20 mg of electrocatalyst in a solution of 50 mL of water containing three drops of 6% PTFE suspension. The resulting mixture was treated in an ultrasound bath for 10 min to obtain a uniform dispersion.

The catalyst slurry was then drop-cast on to a glassy carbon electrode and allowed to dry at 100 ºC for 30 min. For assessing the electrocatalytic activity of the working electrode, cyclic voltammetry was obtained in 1.0 M ethanol and 0.5 M H_2SO_4 solution with a scan rate of 50 mV s^{-1}. For the durability test, the chronoamperometric experiments were carried out at 0.1 V for 2500 s in the same electrolyte. Before each measurement, the solution was purged with high-purity nitrogen gas for at least 30 min to ensure oxygen-free measurements.

5.2.5 Single Cell Test

In the present study, the membraneless ethanol fuel cell (MLEFC) using laminar flow-based fuel cell configuration was fabricated (Arun et al, 2014; Ponmani et al, 2014). In this membraneless fuel cell, ethanol is used as a fuel, sodium perborate is used as an oxidant and seawater is used as an electrolyte. In membraneless fuel cell system seawater used as electrolyte for more accurate that allows both high energy density and low environmental impact at a low cost. In crystalline state sodium perborate exist as a dimeric peroxo-salt with water of hydration, but in aqueous solution affords hydrogen peroxide (Cotton et al, 1988) as shown in Eq. (5.3),

$$[B(OH)_3(O_2H)]^- + H_2O \rightleftharpoons [B(OH)_4]^- + H_2O_2 \qquad (5.3)$$

In MLEFC, the aqueous fuel and oxidant streams flow in parallel in a single microchannel with the anode and cathode on opposing sidewalls (**Fig. 5.1**). Graphite plates of one mm thickness served as current collectors and catalyst support structures. The different anode and cathode catalysts were coated onto the graphite plates. For single cell, the anode catalysts with different atomic ratios were prepared as follows: The catalyst ink was prepared by mixing required quantity of catalyst with a solution of 50 mL of water containing three drops of 6% PTFE dispersion in an ultrasonic bath for 10 min to obtain a uniform dispersion. The catalyst slurry was then spread on the graphite plate by brush and dried at 100 ºC for 30 min to obtain anode and cathode electrodes.

The catalysts tested on the anode side were $Pt_{60}Sn_{30}W_{10}$/VC, $Pt_{60}Sn_{20}W_{20}$/VC, $Pt_{60}Sn_{10}W_{30}$/VC, $Pt_{50}Sn_{50}$/VC, $Pt_{50}W_{50}$/VC and Pt_{100}/VC, Pt with catalyst loading 2 mg/cm^2. On the cathode side, Pt/VC (100) with catalyst loading 2 mg/cm^2 was used in all experiments. The two catalyst-coated graphite plates were aligned to form a channel with 0.1 cm electrode-to-electrode distance (width), a 3 cm length, and a 0.1 cm height. The anolyte (fuel and electrolyte) and catholyte (oxidant and seawater) streams flow in a laminar fashion over the anode and cathode, respectively.

The electrode area along a microchannel wall between the inlets and the outlet (3 cm long and 0.1 cm wide) was used as the geometric surface area of the electrodes in this study (0.3 cm^2). The design is described in detail elsewhere (Choban et al, 2004; Jayashree et al, 2010). The anolyte used in the anode side was 1.0 M ethanol + 0.5 M H_2SO_4 and the catholyte used in the cathode side was 0.1 M perborate in seawater. The flow rate of each of the streams was 0.3 mL min^{-1} (total flow rate of 0.6 mL min^{-1}). The MLEFC was operated at room temperature. The current-voltage characteristics of

MLEFC were measured using an electrochemical workstation (CH Instruments, model CHI6650, USA) and the data was verified using a multi-meter (MASTECH® MAS830L).

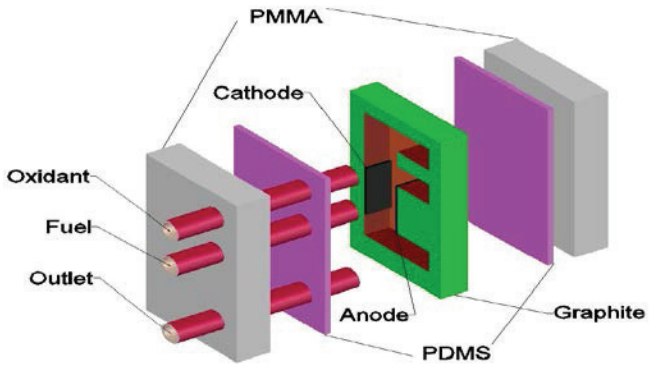

Fig. 5.1 Schematic of the E-shaped membraneless laminar flow based fuel cell with graphite plates molded with poly(dimethylsiloxane) and sealed with poly(methylmethacrylate).

5.3 RESULTS AND DISCUSSIONS

5.3.1 Analysis of Physical Significance

5.3.1.1 XRD – X-Ray Diffraction

XRD analysis was used to establish the atomic structure of the prepared crystalline catalysts. **Fig. 5.2** shows the XRD peaks of Vulcan carbon-support (VC) assisted $Pt_{60}Sn_{30}W_{10}$/VC, $Pt_{60}Sn_{20}W_{20}$/VC, $Pt_{60}Sn_{10}W_{30}$/VC, $Pt_{50}Sn_{50}$/VC, $Pt_{50}W_{50}$/VC and Pt_{100}/VC nanoparticles. For all the synthesized catalysts, the wide peak obtained between 25 and 30^o is affiliated with the zero-zero-two plane of the six-membered hexagon architecture for carbonaceous supports. Together with, peaks of 2θ appearing at 39.1°, 47.4°, 68.5° and 81.8° are analogous of significant planes of 111, 200, 220, and 311 relevant to the unique face-centered-cubic (FCC) nature of metallic platinum. No

additional peaks related to SnO_2 are displayed. The XRD patterns of the prepared catalysts showed that all the diffraction peaks were apparently shifted to higher 2θ values with respect to the corresponding peaks of the platinum catalyst, indicating an interlace augmentation arising from the incorporation of the second and third atoms into the Pt lattice due to the formation of VC-support assisted Pt–Sn–W alloy nanoparticles.

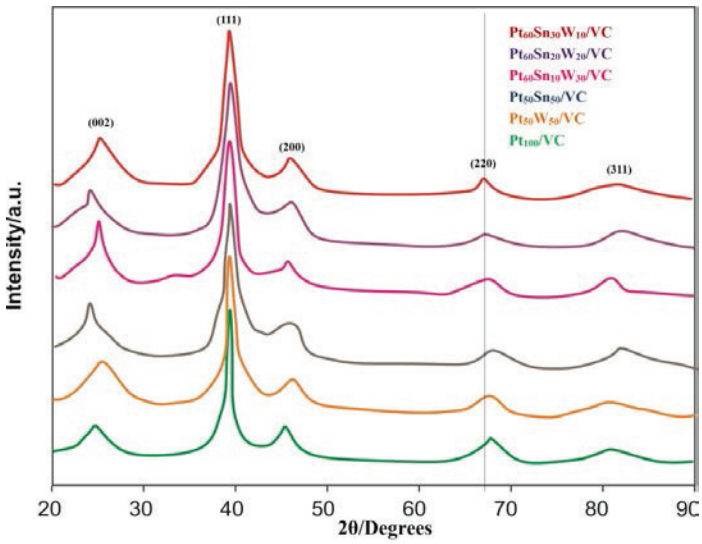

Fig. 5.2 X-ray diffraction peaks of $Pt_{60}Sn_{30}W_{10}$/VC, $Pt_{60}Sn_{20}W_{20}$/VC, $Pt_{60}Sn_{10}W_{30}$/VC, $Pt_{50}Sn_{50}$/VC, $Pt_{50}W_{50}$/VC and Pt_{100}/VC alloy nanoparticles.

The XRD patterns of Pt–Sn–W/VC nanoparticles do not illustrate any peaks of tungsten or tungsten oxides. Despite their characteristic appearance cannot be ruled out, because the tungsten particles probably exist in smaller size or present in an amorphous form. The Scherrer's formula is used to calculate the average particle size of the $Pt_{60}Sn_{30}W_{10}$/VC, $Pt_{60}Sn_{20}W_{20}$/VC, $Pt_{60}Sn_{10}W_{30}$/VC, $Pt_{50}Sn_{50}$/VC, $Pt_{50}W_{50}$/VC and Pt_{100}/VC alloy nanoparticles prepared with the platinum content. The average size of Pt-W/VC, Pt-Sn/VC as well as Pt-Sn-W/VC nanoparticles is smaller than that of the Pt/VC prepared with the similar procedure shown in **Table 5.1.**

Table 5.1 The composition and particle size of synthesized nanoparticles.

Nanoparticles	Initial-atomic ratio (nm)			Estimated atomic ratio (nm)			Structural lattice periodicities (nm)	Average crystalline size (nm)	TEM nanoparticle size (nm)
	Pt	Sn	W	Pt	Sn	W			
Pt_{100}/VC	100	-	-	97	-	-	0.3915	4.5	4.1
$Pt_{50}W_{50}$/VC	50	-	50	53	-	47	0.3905	4.4	4.1
$Pt_{50}Sn_{50}$/VC	50	50	-	52	48	-	0.3887	3.7	3.5
$Pt_{60}Sn_{10}W_{30}$/VC	60	10	30	63	8	29	0.3904	3.7	3.4
$Pt_{60}Sn_{20}W_{20}$/VC	60	20	20	63	19	18	0.3896	3.5	3.3
$Pt_{60}Sn_{30}W_{10}$/VC	60	30	10	62	28	10	0.3899	3.2	3.1

5.3.1.2 TEM–Transmission Electron Microscopy

TEM-Transmission electron microscopy experiments be executed in order to investigate the particle sizes concerning Vulcan carbon-support assisted Pt−Sn−W alloy nanoparticles. **Fig. 5.3** shows the prototypical transmission electron microscopy illustrations of the synthesized platinum alloy nanoparticles. TEM images reveal that the metal particles are nanosized and evenly transfused on VC. Further, TEM images clearly show that each individual catalysts are spherical in shape and having the size of below five nanometers with slight agglomeration. The reason for agglomeration is due to the rapid reduction process of the metal-salt-precursors. As a matter of fact, the dissemination of the synthesized nanoparticles is confined towards systematically for certain range. Consequently, the dispersion of nanoparticles on TEM analysis was

carried out by widely choosing proportionate number of particles related to each TEM illustrations.

Correspondingly, the size of nanoparticles obtained is between 3.1 and 4.1 nanometers, with an average diameter of 3.3 nm for Pt−Sn−W/VC, nanoparticles. Moreover, the TEM illustrations witnessed that the proportions of Pt−Sn−W/VC nanoparticles were lesser than that of the binary Pt−Sn/VC as well as Pt−W/VC nanoparticles.

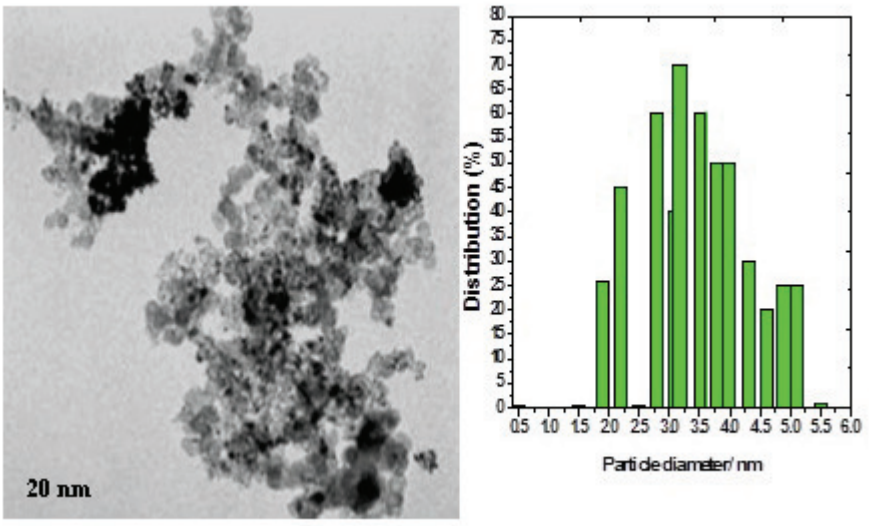

Fig. 5.3 Illustrations of transmission electron microscopy and its histograms of Pt/Sn/W-alloyed nanoparticles on VC support.

5.3.1.3 EDX – Energy Dispersive X-ray Microanalysis

EDX is a powerful method to characterize the chemical composition and texture concerning Pt−Sn−W nanoparticles supported on Vulcan carbon. The EDX spectra shown in **Fig. 5.4** inveterate the presence of Pt, Sn, W nanoparticles along with amorphous carbon. The EDX results are exhibited in **Table 5.1**. A minimum variation of the atomic ratio is observed in the prepared catalysts with the desired elements.

Meanwhile, the experimental values achieved from EDX are having the acceptable agreement with the formal value.

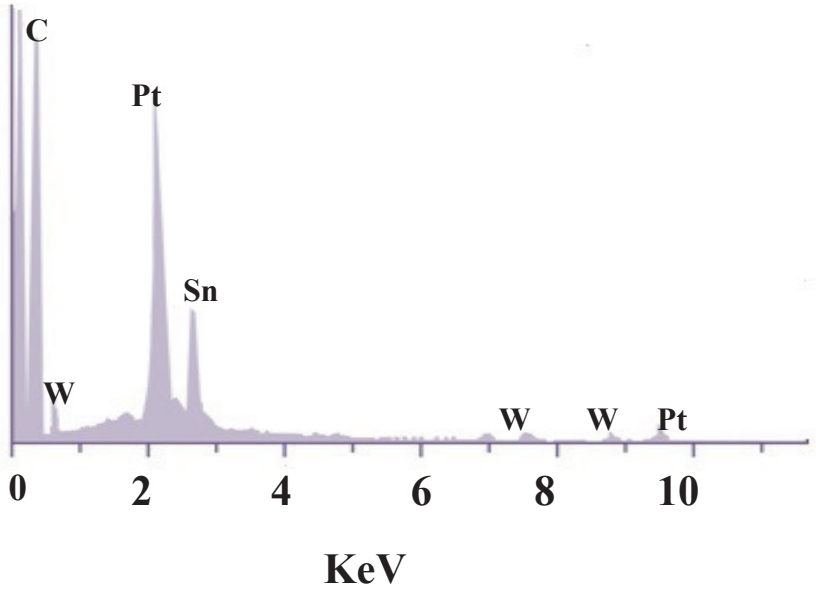

Fig. 5.4 Spectrum of Energy Dispersive X-ray Analysis for Pt−Sn−W/VC nanoparticles.

5.3.2 Analysis of Electrochemical Significance

5.3.2.1 CV – Cyclic voltammetry

In the present study, cyclic voltammetry is used to characterize the electrode mechanism involved in the nanoparticles synthesized by thermal reduction method. **Fig. 5.5-(a)** displays the cyclic voltammograms of $Pt_{60}Sn_{30}W_{10}$/VC, $Pt_{60}Sn_{20}W_{20}$/VC, $Pt_{60}Sn_{10}W_{30}$/VC, $Pt_{50}Sn_{50}$/VC, $Pt_{50}W_{50}$/VC and Pt_{100}/VC nanoparticles applied on the surface of the glassy carbon electrode in the presence of the electrolyte. Consequently, voltammogram representations of the electro-catalysts do not stimulate a legible hydrogen adsorption as well as desorption region (up to 40 mV) usually as observed in platinum metal particles.

However, the current for all the bimetallic and trimetallic catalysts in the double-laminar-range (from 40 to 80 mV *versus* RHE) is more related to monometallic platinum. In the final analysis, voltammograms activity of all the prepared nanoparticles shows the congruent characteristic of the duplex and triplex doped platinum alloy catalysts incorporating transition elements.

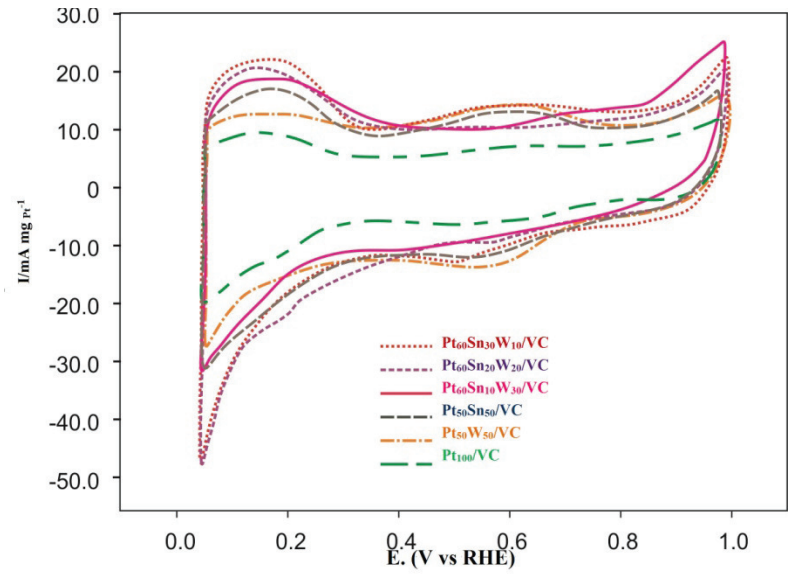

Fig 5.5-(a) Cyclic voltammogram representations of $Pt_{60}Sn_{30}W_{10}$/VC, $Pt_{60}Sn_{20}W_{20}$/VC, $Pt_{60}Sn_{10}W_{30}$/VC, $Pt_{50}Sn_{50}$/VC, $Pt_{50}W_{50}$/VC and Pt_{100}/VC nanoparticles in the absence of fuel.

Subsequently, the out-put values are adjusted into gram per mole of platinum, assuming that alcohol oxidation-reduction reaction appears exclusively onto the reactive sites of platinum at normal temperature.

Fig 5.5-(b) shows the cyclic voltammograms of monometallic Pt_{100}/VC, bimetallic $Pt_{50}W_{50}$/VC and $Pt_{50}Sn_{50}$/VC as well as the trimetallic $Pt_{60}Sn_{30}W_{10}$/VC, $Pt_{60}Sn_{20}W_{20}$/VC and $Pt_{60}Sn_{10}W_{30}$/VC nanoparticles for alcohol oxidation in the presence

of fuel. Consequently, the cyclic voltammograms of platinum alloy nanoparticles for alcohol oxidation represent two oxidation peaks (*versus* RHE), one towards the successive browse while the other involves in the reversal. **Table 5.2** displays the results of cyclic voltammetry in conjunction with the output-voltage and the equivalent current-densities for AOR. Additionally in Fig. 5.5(b), the initial start-up current with respect to AOR on Pt/VC, Pt−W/VC, and Pt−Sn/VC are at about 300 mv vs. RHE.

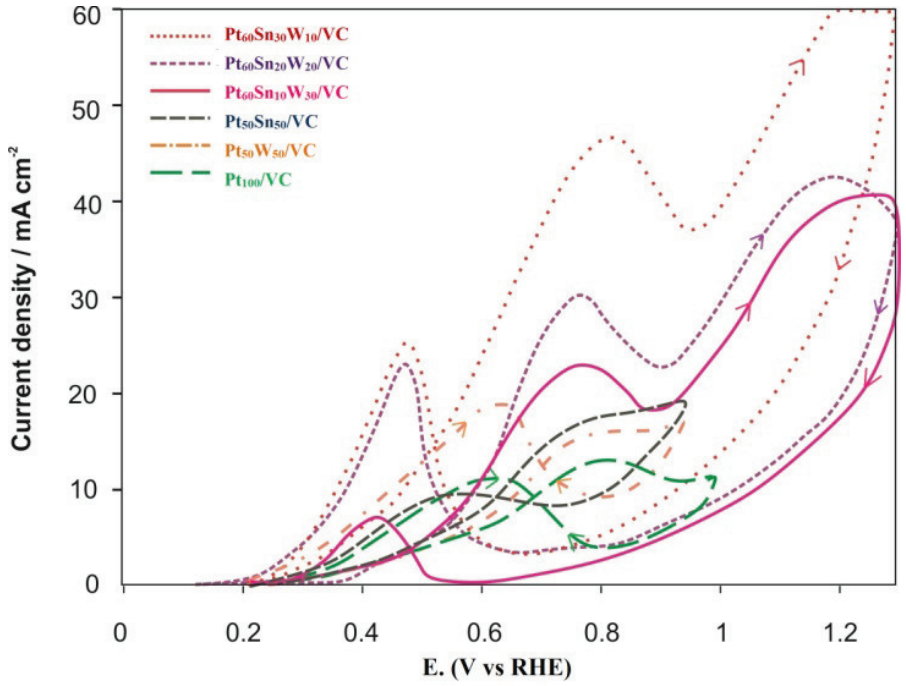

Fig 5.5-(b) Cyclic voltammogram representations of $Pt_{60}Sn_{30}W_{10}$/VC, $Pt_{60}Sn_{20}W_{20}$/VC, $Pt_{60}Sn_{10}W_{30}$/VC, $Pt_{50}Sn_{50}$/VC, $Pt_{50}W_{50}$/VC and Pt_{100}/VC nanoparticles.

At the same time, for tri-metallic Pt−Sn−W/VC catalyst, the start-up voltage for alcohol-oxidation advanced to 200 mv vs. RHE, i.e. moved to negativistic-potential closed by 100 mv. Not only the Pt−Sn−W/VC nanoparticles promote the supreme peak-current-density (58.2mA/cm^2) around 0.75 V peak-potential but also executes its best performance in alcohol electro-oxidation compared to the other prepared nanoparticles.

Likewise, Pt/Sn/W nanoparticle on VC support with the composition of (60/30/10) achieves better action than Pt/W-VC and PT/Sn-VC nanoparticles. Significantly, $Pt_{60}Sn_{30}W_{10}$/VC nanoparticle on VC support is an encouraging electrocatalyst for non-membrane fuel cell power systems. Ultimately, the remarkable performance of the triplex Pt−Sn−W/VC nanoparticles empowers the modification of electronic properties of platinum regarding bifunctional mechanism and ligand effect.

Table 5.2 Cyclic voltammetry results of $Pt_{60}Sn_{30}W_{10}$/VC, $Pt_{60}Sn_{20}W_{20}$/VC, $Pt_{60}Sn_{10}W_{30}$/VC, $Pt_{50}Sn_{50}$/VC, $Pt_{50}W_{50}$/VC and Pt_{100}/VC nanoparticles.

Nanoparticles	Scan rate@50 mV/s	
	Maximum output voltage (mV *versus* RHE)	Corresponding current density (mA/cm^2)
Pt_{100}/VC	**795**	**8.5**
$Pt_{50}Sn_{50}$/VC	**823**	**11.9**
$Pt_{50}W_{50}$/VC	**812**	**13.0**
$Pt_{60}Sn_{10}W_{30}$/VC	**740**	**25.2**
$Pt_{60}Sn_{20}W_{20}$/VC	**750**	**32.9**
$Pt_{60}Sn_{30}W_{10}$/VC	**803**	**58.2**

5.3.2.2 CA – Chronoamperometry

The performances on stability and long-term operation tests for $Pt_{60}Sn_{30}W_{10}$/VC, $Pt_{60}Sn_{20}W_{20}$/VC, $Pt_{60}Sn_{10}W_{30}$/VC, $Pt_{50}Sn_{50}$/VC, $Pt_{50}W_{50}$/VC and Pt_{100}/VC nanoparticles

were established by chronoamperometry at 0.80 V for 2000 s. The chronoamperometry results of different electro-catalysts were exhibited in **Fig. 5.6.** It is noted that the initial decrease in current density observed in the first five minutes was due to the attribution of corresponding equilibrium. All things considered, the primary fall-down in current density is resulted to the fresh active surfaces of catalysts against the product of alcohol molecules.

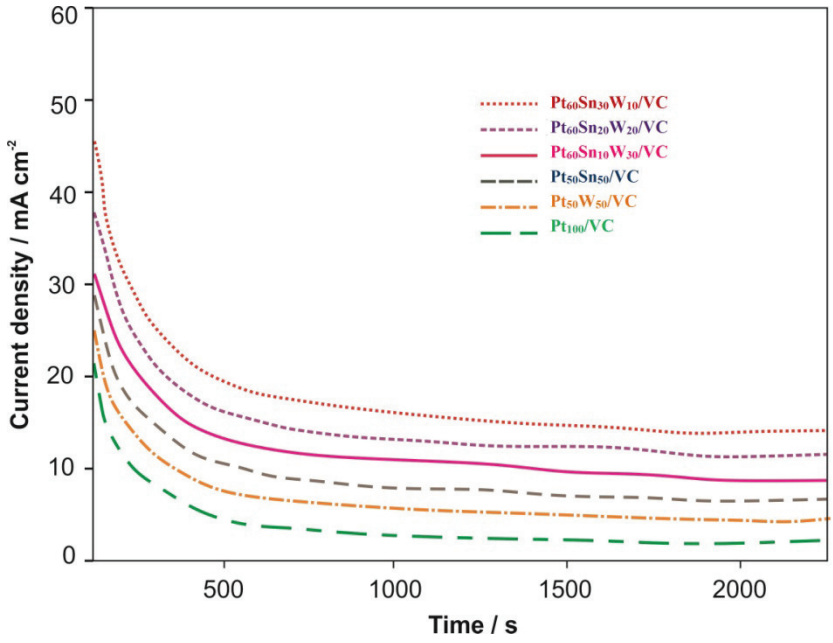

Fig 5.6 Chronoamperometry of $Pt_{60}Sn_{30}W_{10}$/VC, $Pt_{60}Sn_{20}W_{20}$/VC, $Pt_{60}Sn_{10}W_{30}$/VC, $Pt_{50}Sn_{50}$/VC, $Pt_{50}W_{50}$/VC and Pt_{100}/VC nanoparticles at room temperature.

However, in the process of oxidoreduction, the rate of assimilation of fuel molecules rely upon the possibility of freshly available reactive sites of the catalysts. Subsequently, the indicated catalytic reliant process is faster as a consequence to stimulate the oxidation of intermediate species with an acceptable competency. Therefore, the catalytic surface becomes unstable due to crystallization, segregation as well as hard deposits of intermediate molecules to form a fresh active sites of electro-catalysts.

Although the profitable outcome of W incorporation, have been described already for platinum–tin alloy nanoparticles, the first improvement in alcohol oxidation were observed by Calegari et al. 2006; Lim et al. 2009; and Song et al. 2005. In conclusion, the composition and particle size is only the deciding factor for determining the performance of the electro-catalysts.

5.3.3 Assessment of individual cell performance towards seawater electrolysis

Single cell test is used to analyze the activity of the synthesized nanoparticles towards its practical applicability. The electrolytic effect of seawater on Pt_{100}/VC, $Pt_{50}W_{50}$/VC, $Pt_{50}Sn_{50}$/VC, $Pt_{60}Sn_{10}W_{30}$/VC, $Pt_{60}Sn_{20}W_{20}$/VC and $Pt_{60}Sn_{30}W_{10}$/VC nanoparticles were studied in a single non-membrane fuel cell power system for alcohol oxidation. Correspondingly, the combined plot of potential, as well as power density, versus current density has been displayed in **Fig. 5.7.** Though protonated acid has been depleted as the electrolyte, electrolysis towards alcohol oxidation was poor as compared to seawater. Consequently, this behavior was mainly assigned to the electro generation of seawater towards alcohol oxidation. As shown below, the results of single cell test performed on various synthesized electrocatalysts have been concluded and tabulated (**Table 5.3**).

Additionally, it has been observed that the efficiency of tungsten fused with platinized tin nanoparticles on VC support achieved more excellent results than the activity of other catalysts. The utmost power-density of 37.9 mW/cm^2 is gained at the trimetallic Pt, tin, and W catalyst. Moreover, the observation of electrogeneration in seawater indicated uniquely that the presence of a fractional quantity of W associated with tungsten doped platinized-tin on VC nanoparticles is the reason for the acceleration of AOR.

Table 5.3 Analysis of individual cell performance towards seawater electrolysis.

Nanoparticles	Potential (V)	Highest power-density (mW/cm^2)	Highest current-density (mA/cm^2)
Pt_{100}/VC	0.52	6.0	48.3
$Pt_{50}W_{50}/VC$	0.61	18.8	85.1
$Pt_{50}Sn_{50}/VC$	0.69	26.2	106.3
$Pt_{60}Sn_{10}W_{30}/VC$	0.76	28.6	155.7
$Pt_{60}Sn_{20}W_{20}/VC$	0.80	31.7	190.2
$Pt_{60}Sn_{30}W_{10}/VC$	0.85	37.9	210.3

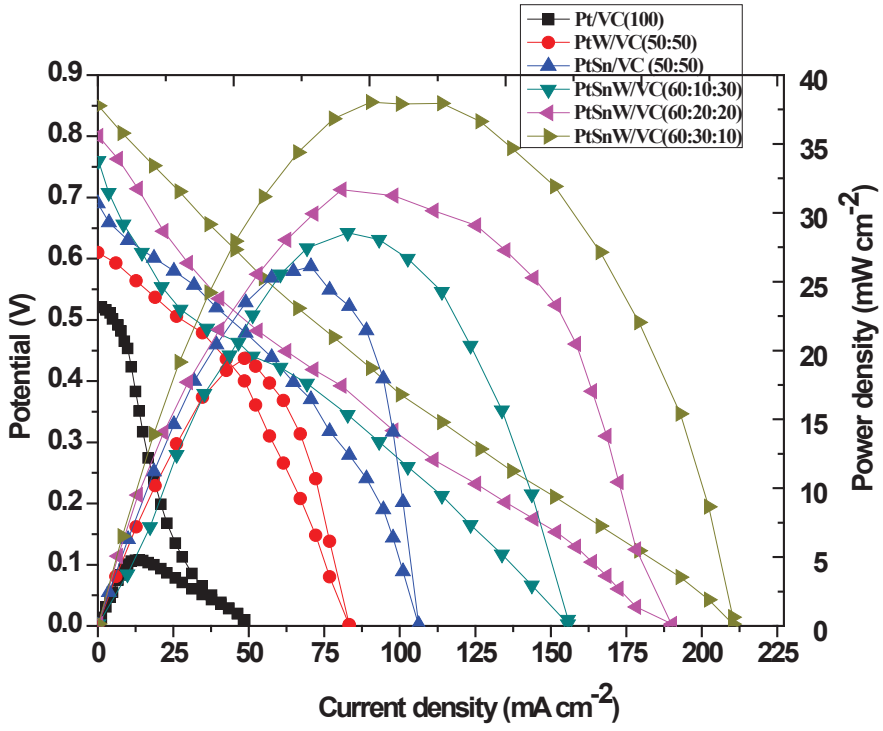

Fig 5.7 Potential as well as power density versus current density curves for Pt_{100}/VC, $Pt_{50}W_{50}/VC$, $Pt_{50}Sn_{50}/VC$, $Pt_{60}Sn_{10}W_{30}/VC$, $Pt_{60}Sn_{20}W_{20}/VC$ and $Pt_{60}Sn_{30}W_{10}/VC$ nanoparticles.

In like manner, Ribeiro et al. (2007) also discovered comparable observations towards alcohol oxidation in the presence of platinum alloy catalysts by various catalyst preparation methods. Apparently, it is concluded that the inception of seawater onto the tungsten doped platinized tin nanoparticles on VC support improved the performance of non-membrane fuel cell power systems by way of reducing the depletion boundary layer.

5.4 CONCLUSIONS

In this work, the study of ethanol oxidation on seawater-supported Pt–Sn–W/VC ternary electrocatalysts has revealed details concerning the activity and stability of the catalysts in membraneless fuel cells. The maximum activity for ethanol oxidation was found for the $Pt_{60}Sn_{30}W_{10}$/VC than the $Pt_{60}Sn_{20}W_{20}$/VC, $Pt_{60}Sn_{10}W_{30}$/VC, $Pt_{50}Sn_{50}$/VC, $Pt_{50}W_{50}$/VC and Pt_{100}/VC due to the supportive electrogeneration of seawater. The significantly enhanced catalytic activity for ethanol oxidation can be attributed to the high dispersion of ternary catalysts and to W acting as a promotion agent. XRD results show the homogenous alloy structure of Pt, Sn and W. The TEM images indicated an average size of ternary nanoparticles of 3-4 nm. The atom ratio of Pt, Sn and W from EDX analysis is close agreement with the original precursor concentration. The composition of ternary nanoparticles can be conveniently controlled by adjusting the initial metal salt solution and preparation conditions. The electrochemical experiments showed that the $Pt_{60}Sn_{30}W_{10}$/VC electrocatalysts have higher catalytic activity than that of the other catalysts. The enhancements in activity and stability over Pt–Sn–W/VC catalyst have been solely attributed to the development of additional electrogeneration in seawater.

REFERENCES

1) **Adamson KA, Pearson P, 2000,** 'Hydrogen and methanol: a comparison of safety, economics, efficiencies and emissions', *J. Power Sources*, Vol.86, p.548.

2) **Ahn SH, Kwon OJ, Kim SK, Choi I, Kim JJ, 2010,** 'Electrochemical preparation of Pt-based ternary alloy catalyst for direct methanol fuel cell anode', *Int. J. of Hydrogen Energy*, VolS.35, p.13309–13316.

3) **Arun A, Gowdhamamoorthi M, Kiruthika S, Muthukumaran B, 2014,** 'Electrochemical characterization of Pt-Ru-Ni/C anode electrocatalyst for methanol electrooxidation in membraneless fuel cells', *J. Electrochem. Soc,* Vol. 161, p. F311.

4) **Beden B, Lamy C, Bewick A, Kunimatsu K, 1981,** 'Electrosorption of methanol on a platinum electrode. IR spectroscopic evidence for adsorbed CO species', *J. Electroanal. Chem.* Vol.121, p.343.

5) **Beyhan S, Leger JM, Kadirgan F, 2013,** 'Pronounced synergetic effect of the nano sized PtSnNi/C catalyst for ethanol oxidation in direct ethanol fuel cell', *Appl. Catal. B Environ*. Vol.130, p.305–313.

6) **Biegler T, Rand DAJ, Woods R, 1971,** 'Limiting oxygen coverage on platinized platinum; Relevance to determination of real platinum area by hydrogen adsorption', *J. Electroanal. Chem. Interfacial Electrochem*, Vol.29, p.269–277.

7) **Bonesi AR, Moreno MS, Triaca WE, Luna AMC, 2010,** 'Modified catalytic materials for ethanol oxidation', *Int. J. Hydrogen Energy*, Vol.35, p.5999–6004.

8) **Bonesi A, Asteazaran M, Moreno MS, Zampieri G, Bengio S, Triaca W, Castro Luna AM, 2013,** 'Preparation and evaluation of carbon supported catalysts for ethanol oxidation', *J. Solid State Electrochem*, Vol.17, p.1823.

9) **Burnstein GT, Barnett CJ, Kucernak AR, Williams KR, 1997,** 'Aspects of anodic oxidation of methanol', *Catalysis Today*, Vol.38, p.425.

10) **Cao J, Du C, Wang SC, Mercier P, Zhang X, Yang H, 2007,** 'The production of a high loading of almost monodispersed Pt nanoparticles on single walled carbon nanotubes for methanol oxidation', *Electrochem. Commun*. Vol.9, p.735–740.

11) **Chan KY, Ding J, Ren J, Cheng S, Tsang KY, 2004,** 'Supported mixed metal nanoparticles as electrocatalysts in low temperature fuel cells', *J. Mater. Chem*., Vol.14, p.505.

12) **Choban ER, Markoski LJ, Wieckowski A, Kenis PJA, 2004,** 'Microfluidic fuel cell based on laminar flow', *J. Power Sources*, Vol. 128, p.54.

13) **Choi WC, Woo SI, 2003,** 'Bimetallic Pt-Ru nanowire network for anode material in a direct-methanol fuel cell', *J. Power Sources*. Vol.124, p.420–425.

14) **Colmati F, Antolini E, Gonzalez ER, 2007,** 'Ethanol oxidation on a carbon – supported $Pt_{75}Sn_{25}$ electrocatalyst prepared by reduction with formic acid: Effect of thermal treatment', *Appl. Catal. B*, Vol.73, p.106.

15) **Cotton FA, Wilkinson G, 1998,** Wiley Interscience, New York, p. 812.

16) **Gasteiger HA, Markovic N, Ross PN, Cairns EJ, 1993,** 'CO electrooxidation on well characterized Pt – Ru alloys', *J. Phys. Chem*., Vol.97, p.12020–12029.

17) **Gowdhamamoorthi M, Arun A, Kiruthika S, Muthukumaran B, 2014,** 'Perborate as novel fuel for enhanced performance of membraneless fuel cells', *Ionics*. Vol.20, p.1723–1728.

18) **Hamnett A, 1997,** 'Mechanism and electrocatalysis in the direct methanol fuel cell', *Catalysis Today*, Vol.38, p.445.

19) **Hart D, Leach MA, Fouquet R, Pearson PJ, Bauen A, 2000,** 'Methanol infrastructure-will it affect the introduction of SPFC vehicles?', *J. Power Sources*, Vol.86, p.542.

20) **Jayashree RS, Yoon SK, Brushett FR, Lopez Montesinos PO, Natarajan D, Markoski LJ, Kenis PJA, 2010,** 'On the performance of membraneless laminar flow-based fuel cells', *Journal of Power Sources*, Vol.195, p.3569.

21) **Kiso F, Arashi N, 1998,** 'Hybrid Methanol production process', *Applied Energy*, Vol.59, p.215.

22) **Lamy C, Rousseau S, Belgsir E, Coutanceau C, Léger JM, 2004,** 'Recent progress in the direct ethanol fuel cell: Development of new platinum–tin electrocatalysts', *Electrochim Acta,* Vol. 49, p.3901–3908.

23) **McNicol BD, Rand DAJ, Williams KR, 1999,** 'Direct methanol air fuel cells for road transportation' *J. Power Sources*, Vol.83, p.15.

24) **Moreno B, Jurado JR, Chinarro E, 2009,** 'Pt-Ru-Co catalysts for PEMFC synthesized by combustion, *Catalysis Communications*, Vol.11, p.123–126.

25) **Pechini PM, 1967,** Unites States Patent Office, 3330697.

26) **Ponmani K, Durga S, Arun A, Kiruthika S, Muthukumaran B, 2014,** 'Development of membraneless sodium perborate fuel cell for media flexible power generation', *International Journal of Electrochemistry*, Vol.14, p.1.

27) **Radmilovic V, Gasteiger HA, Ross PN, 1995,** 'Structure and chemical composition of a supported Pt–Ru electrocatalysis for methanol oxidation', *J. Catal*. Vol.154, p.98–106.

28) **Rivera EC, Volpe DJ, Alden L, Lind C, Downie C, Vazquez-Alvarez T, 2004,** 'Electrocatalytic activity of ordered intermetallic phases for fuel cell applications', *J. Am. Chem. Soc*., Vol.126, p.4043–4049.

29) **Ribeiro J, dos Anjos DM, Kokoh KB, Coutanceau C,Leger JM, Olivi P, de Andrade AR, Tremiliosi-Filho G, 2007,** 'Carbon supported ternary PtSnIr catalysts for direct ethanol fuel cell', *Electrochimica Act,* Vol.52, p.6997.

30) **Vigier F, Coutanceau C, Hahn F, Belgsir EM, Lamy C, 2004,** 'On the mechanism of ethanol electro-oxidation on Pt and PtSn catalysts: Electrochemical and in situ IR reflectance spectroscopy studies', *J.Electroanal. Chem,* Vol. 563, p.81-89.

31) **Vigier F, Coutanceau C, Perrard A, Belgsir E, Lamy C, 2004,** 'Development of anode catalysts for a direct ethanol fuel cell', *J. Appl. Electrochem*. Vol.34, p.439–446.

32) **Xiong L, Kannan A, Manthiram A, 2002,** 'Pt-M(M= Fe, Co, Ni and Cu electrocatalysts synthesized by an aqueous route for proton exchange membrane fuel cells', *Electrochem. Commun*., Vol.4, p.898–903.

33) **Yajima T, Uchida H, Watanabe M, 2004,** 'In-situ ATR-FTIR spectroscopic study of electro oxidation of methanol and adsorbed CO at Pt-Ru alloy', *J. Phys. Chem. B*. Vol.108, p.2654–2659.

34) **Zhou Z, Wang S, Zhou W, Wang G, Jiang L, Li W, 2003,** 'Novel synthesis of highly active Pt/C cathode electrocatalyst for direct methanol fuel cell', *Chem. Commun*. P.394–395.